Available online at www.sciencedirect.com
ScienceDirect
Medical Engineering & Physics 30 (2008) 358–366
Medical Engineering & Physics
www.elsevier.com/locate/medengphy

Experimental measurement and modeling analysis on mechanical properties of tensor tympani tendon

Tao Cheng, Rong Z. Gan *

School of Aerospace and Mechanical Engineering, Bioengineering Center, University of Oklahoma, Norman, OK 73019, United States

Received 27 October 2006; received in revised form 5 April 2007; accepted 5 April 2007

Abstract

In this paper, we report mechanical properties of the tensor tympani tendon of human ear measured from uniaxial tensile, stress relaxation and failure tests. The hyperelastic Ogden model and digital image correlation method were employed to analyze experimental data. The constitutive equation of the tendon was derived through data iteration processes, and Young's modulus was presented as a function of stress. The viscoelastic property of the tendon was described by stress relaxation function and hysteresis. Furthermore, three-dimensional finite element analysis was carried out on five tendon models to investigate relationship between the structure and properties. The dimensions of the tendon were also measured by image processing techniques and presented with statistic significance. The structure and properties of the tensor tympani tendon reported in this study add new data into the study of ear tissue biomechanics.

Keywords: Tensor tympani tendon; Mechanical properties; Finite element modeling; Tissue biomechanics

1. Introduction

The tensor tympani tendon of human middle ear lies between cochleariform process of the bony wall and neck of the malleus in the middle ear cavity (Fig. 1). The tensor tympani muscle is connected to the tendon directly. The muscle contraction increases the tension on the tympanic membrane (TM) through the tendon, which is important since a loose TM will not be able to transmit the vibration effectively to the ossicles [1,2]. In clinics, tonic contraction of the tensor tympani muscle may cause non-specific ear symptoms, such as fullness, tinnitus, slight hearing loss or Meniere's disease-like findings [3–5]. In middle ear reconstruction, it is necessary to reconstruct the tensor tympani tendon for a successful restoration of sound conduction [6,7]. The tensor tympani tendon is also pathologically involved in inflammatory process of otitis media which may affect the acoustic reflex process [8]. Therefore, understanding the structure and properties of the tensor tympani tendon is important for the study of normal and pathological functions of middle ear.

Mechanical properties of the tensor tympani tendon have not been reported in literature, and this deficiency directly affects fully understanding of middle ear mechanics for sound transmission. Moreover, in developing an accurate finite element model of human ear, geometric characterization and mechanical properties of the tensor tympani tendon are required [9].

A variety of mechanical tests have been reported to measure properties of soft tissues, such as uniaxial tensile [10], strip biaxial tension [11], and shear tests [12]. Among them, the uniaxial tensile test is commonly used to characterize one-dimensional tensile properties of ligament tissues [13] and was employed in this study. Soft tissues usually show viscoelastic behavior in their physiological function range [14]. The stress relaxation and failure tests were carried out to determine viscoelastic properties and ultimate stress and strain of the tendon.

In addition to experimental measurement, numerous material models have been developed to simulate the behavior of tissues in analytical ways. Weiss et al. [15] used a hyperelastic material model with an exponential strain energy

* Corresponding author at: Biomedical Engineering, School of Aerospace and Mechanical Engineering, University of Oklahoma, 865 Asp Avenue, Room 200, Norman, OK 73019, United States. Tel.: +1 405 325 1099; fax: +1 405 325 1088.
E-mail address: rgan@ou.edu (R.Z. Gan).

1350-4533/$ – see front matter © 2007 IPEM. Published by Elsevier Ltd. All rights reserved.
doi:10.1016/j.medengphy.2007.04.005

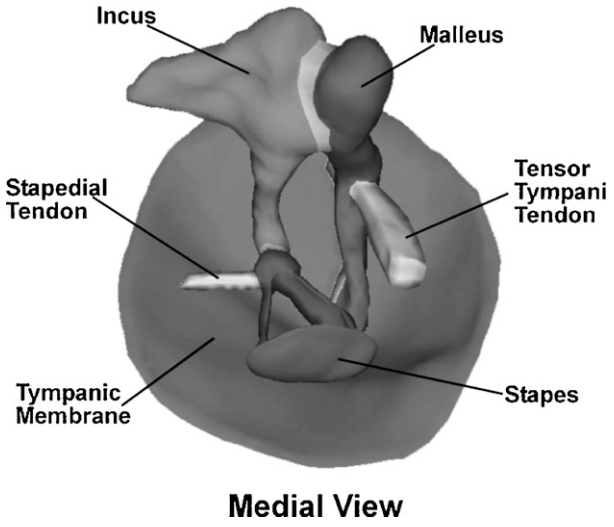

Fig. 1. Medial view of a left human middle ear model with the tensor tympani tendon.

function to fit experimental curves of human medial collateral ligament through finite element (FE) analysis. Liu et al. [16] applied a nonlinear Arruda-Boyce model to simulate soft tissues undergoing large indentations. There are several nonlinear hyperelastic material models available for analyzing mechanical properties of biological soft tissues, such as the Ogden, Mooney-Rivlin and Yeoh models. In this study, we used the Ogden model to analyze behavior of the tensor tympani tendon under the uniaxial tensile test and investigated the relationship between the structure and properties of the tendon by FE modeling.

2. Methods

2.1. Specimen preparation

Ten tensor tympani tendon specimens were harvested from fresh frozen human temporal bones through the Willed Body Program at University of Oklahoma Health Sciences Center. The donors' ages were from 50 to 85 years old, three males and seven females. All the experiments were performed within 6 days after obtaining the bones. The specimen was prepared with the malleus and cochleariform attached as shown in Fig. 2A. Two bony ends were trimmed and attached to the mounting fixture under the microscope (Olympus SZX12) by cyanoacrylate glue. The fixture has two pre-aligned metal plates to hold the specimen along the longitudinal direction. Care was taken to avoid distortion of the specimen during this process. The metal plates were then connected by two plastic adapters and mounted to the material testing system (MTS, TestResources, MN) as a whole unit. A ruler was attached to the upper metal plate as a dimensional reference (Fig. 2B). After the specimen was lined up with grips in MTS, plastic adapters were removed and a preload of 0.001 N was applied to the specimen through the load cell to adjust the zero load state. The still images of the tendon in front and side views were captured at the initial state using a digital CCD camera attached to a surgical microscope (OPMI 1-FC, Zeiss). The tendon was distinguished from bony ends in the image to measure initial dimensions through the Measuring Tools in Adobe Photoshop 7.0 at a resolution of 0.01 mm. The length, width, and thickness of specimens are listed in Table 1, with mean and standard deviation (S.D.).

2.2. Mechanical testing

The MTS with SMT1-2.2lbs load cell (Interface, Inc.) was used to measure load and deformation data of the specimen during the test. The displacement was applied to the bottom part of the specimen, and the top part was fixed (Fig. 2B). A preconditioning was performed on each specimen at the beginning [14], with five cycles of uniaxial elongation at the elongation rate of 0.1 mm/s and stretching of 10% of the original length. Repeated loading–unloading curves were gradually decreasing and a steady state was gen-

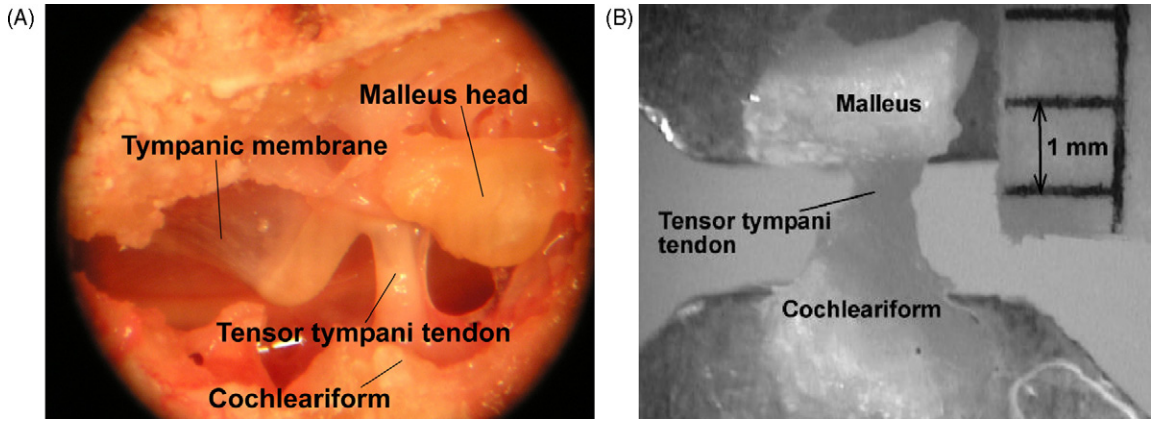

Fig. 2. (A) The tensor tympani tendon in middle ear cavity connecting to the malleus head and cochleariform was viewed in a human cadaver temporal bone. (B) The tensor tympani tendon specimen was fixed at the mounting fixture along the longitudinal direction in material testing system (MTS). A ruler was attached to the metal holder at the load cell side as a dimensional reference.

Table 1
Dimensions of tensor tympani tendon (TTT) specimens ($N = 10$)

	TTT1	TTT2	TTT3	TTT4	TTT5	TTT6	TTT7	TTT8	TTT9	TTT10	Mean	S.D. (±)
Length (mm)	1.23	1.27	1.58	1.44	1.59	1.79	1.51	1.25	1.39	1.45	1.45	0.18
Width (mm)	1.14	0.97	1.39	1.46	1.23	1.26	1.10	0.96	0.90	0.82	1.12	0.21
Thickness (mm)	0.50	0.57	1.00	1.05	1.58	1.05	0.47	0.88	1.10	0.67	0.84	0.43

erally observed after the third cycle as shown in Fig. 3. After preconditioning, the specimen was subjected to following tests under the uniaxial tensile test setup. Note that at the end of each test, the specimen was returned to the initial unstressed state and enough time (2–3 min) was given for the recovery from previous deformation. The images of the deformation process were recorded simultaneously using the digital CCD camera with a frame rate of 30 frames/s.

2.2.1. Uniaxial tensile test

The elongation rate was set at 0.01 mm/s and stretching at 40% of the original length. Three parameters: load, deformation and time, were recorded with a resolution level of 10^{-6} N in force, and 10^{-6} mm in displacement.

2.2.2. Stress relaxation test

An approximate step function of elongation was applied to the specimen at the beginning ($t = 0$) with the elongation rate of 1.8 mm/s and stretching of 40% of the original length. The corresponding stress including the initial stress response σ_0 and relaxed stress $\sigma(t)$ were recorded over a period of time until the rate of loading change was less than 0.1%/s, or fully relaxed. The MTS data recording program was then stopped manually and the specimen was returned to the initial unstressed state.

2.2.3. Failure test

The elongation rate was set at 0.02 mm/s. The specimen was stretched till it was broken. The entire failure process was recorded using the CCD camera and the breaking site of each specimen was observed.

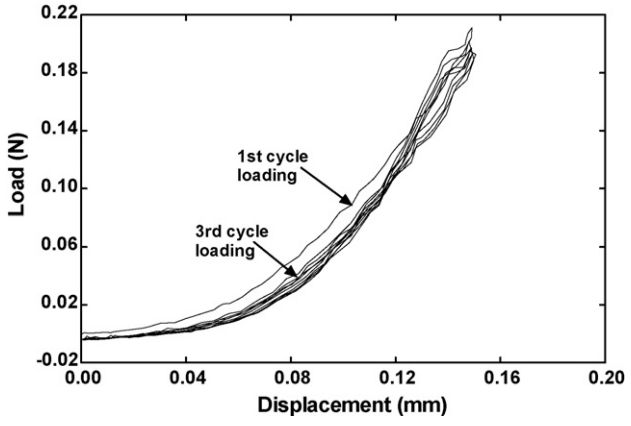

Fig. 3. The preconditioning process (five cycles) of a tensor tympani tendon specimen recorded in MTS.

Note that all the specimens were maintained in their physiological conditions by spraying normal saline solution to back side (opposite to the camera) of the tissue during the test.

2.3. Digital image correlation method

It is important to verify effects of boundary conditions on mechanical testing of tissues with small dimensions. The digital image correlation (DIC) method, a non-contact method for measuring the surface displacement or strain distribution, was employed based on images simultaneously recorded during the uniaxial tensile test. In DIC, the deformation of the specimen was computed by the existence of a distinct gray-scale pattern of pixels on the image. Three steps were employed to achieve the DIC algorithm: displacement mapping, bicubic spline interpolation, and least squares correlation (see Lu and Cary [17] for a detail explanation of the DIC algorithm).

All the images were first digitized using Adobe Premiere 6.5 and output as sequential images at a constant time interval, starting from time $t = 0$ to the end of loading. The first image was used as a reference and the consecutive images were used as deformed images. Fig. 4 shows one reference and three consecutive images of a tendon specimen. The horizontal and vertical lines were drawn in the reference image within a relatively large area around the center of the specimen in DIC software (WinDIC_LS 2.0, provided by Professor Lu at Oklahoma State University). A grid of nodes was then generated along these lines and deformation was calculated at each node by tracing displacement of nodes in deformed images. The normal strain ε in loading direction was then calculated as $\varepsilon = (L - L_0)/L_0$, where L_0 is the original length of vertical lines at time $t = 0$, and L is the length of each vertical line at time t. The average strain were then derived and synchronized with the stress measured by the load cell. The stress–strain relationship based on DIC analysis was further compared with that obtained from the experiment.

2.4. Data analysis for viscoelasticity

The MTS experimental data were post-processed to obtain the stress–strain relationship and Young's modulus–stress relationship of the tensor tympani tendon. In literature, the Ogden model has been well used to predict the behavior of nonlinear and viscoelastic soft tissues such as the skin [18], muscle [19] and brain tissue [20], and was employed in this study.

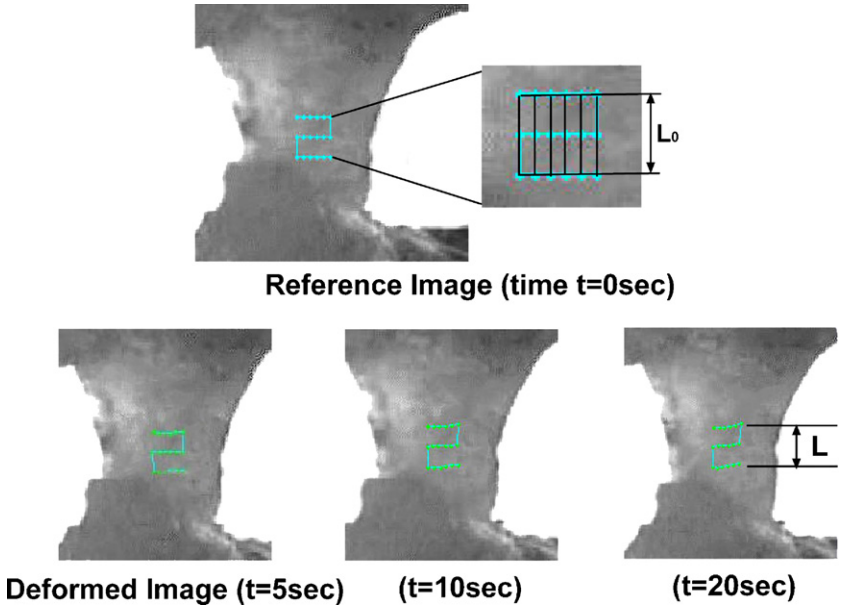

Fig. 4. Illustration of digital image correlation (DIC) method for calculating the strain distribution of the tensor tympani tendon specimen under the loading process. The image of the tendon at time $t=0$ was used as a reference image and three images of the tendon at three time intervals ($t=5$, 10 and 20 s) were used as deformed images. A grid was generated at the middle portion of the reference image and horizontal and vertical lines were identified. The length of the vertical line in the reference image is measured as the original length (L_0) of the specimen and the length of the vertical line in deformed images is the deformed length (L) of the specimen.

For uniaxial elongation, the Ogden model is generally expressed as

$$\sigma = \frac{2\mu_1}{\alpha_1}[(1+\varepsilon)^{\alpha_1-1} - (1+\varepsilon)^{-(0.5\alpha_1+1)}] \quad (1)$$

where σ is the normal stress, ε is the strain, and μ_1 and α_1 are material constants [21]. In this paper, we used the stretch ratio λ, the ratio of deformed length to original length, to describe the strain and $\varepsilon = \lambda - 1$, thus, Eq. (1) becomes

$$\sigma = \frac{2\mu_1}{\alpha_1}[\lambda^{(\alpha_1-1)} - \lambda^{-(0.5\alpha_1+1)}] \quad (2)$$

Differentiating Eq. (2) with respect to λ, we had the tangent modulus or Young's modulus $d\sigma/d\lambda$

$$\frac{d\sigma}{d\lambda} = \frac{2\mu_1}{\alpha_1}\left[(\alpha_1-1)\lambda^{\alpha_1-2} + \left(\frac{\alpha_1}{2+1}\right)\lambda^{-(0.5\alpha_1+2)}\right] \quad (3)$$

The material constants (μ_1 and α_1) were derived from stress–strain curves of specimens in tensile tests through the data iteration process in MATLAB v.7.0., i.e., given experimental data and a user-defined function (Eq. (2) in this study), find coefficients that best fit the function to the data in a least-squares sense. The constitutive equation of the tensor tympani tendon in the Ogden form was then expressed by substituting μ_1 and α_1 into Eq. (2). The Young's modulus $d\sigma/d\lambda$ was derived from Eq. (3).

2.5. Finite element modeling

Since the Ogden model was used in data analysis of raw experimental data, it was selected in FE analysis. The Ogden form of strain energy potential is based on the principal stretches of left-Cauchy strain tensor, which has the form

$$U = \sum_{i=1}^{N}\frac{2\mu_i}{\alpha_i^2}(\bar{\lambda}_1^{\alpha_i} + \bar{\lambda}_2^{\alpha_i} + \bar{\lambda}_3^{\alpha_i} - 3) + \sum_{i=1}^{N}\frac{1}{D_i}(J-1)^{2i} \quad (4)$$

where $\bar{\lambda}_i$'s are deviatoric principal stretches and $\bar{\lambda}_i = J^{-1/3}\lambda_i$, with λ_i's being principal stretches and J the Jacobian determinant of the deformation gradient. N is the number of terms in series, and μ_1's, α_1's, and D_i's are temperature dependent material parameters. The initial shear modulus, G, is given as

$$G = \sum_{i=1}^{N}\alpha_i\mu_i \quad (5)$$

For an incompressible material in the uniaxial stress state, the first-order ($N=1$) Ogden potential can be rewritten as

$$U = \frac{2\mu_1}{\alpha_1^2}(\lambda^{\alpha_1} + 2\lambda^{-0.5\alpha_1} - 3) \quad (6)$$

The derivative of Eq. (6) with respect to λ leads to the same constitutive equation as Eq. (2).

A parallel-bundled fibrous microstructure of the tensor tympani tendon (Fig. 5A) was observed using the scanning electron microscope (SEM, Model: DSM960, Zeiss) with 3000× magnification in Samuel Roberts Noble Electron Microscopy Lab at University of Oklahoma. Based on that, five 3D FE models of the tendon with different fiber to ground substance volume ratio (k) values were created in ANSYS v.10.0 (ANSYS Inc., Canonsburg, PA) as shown in

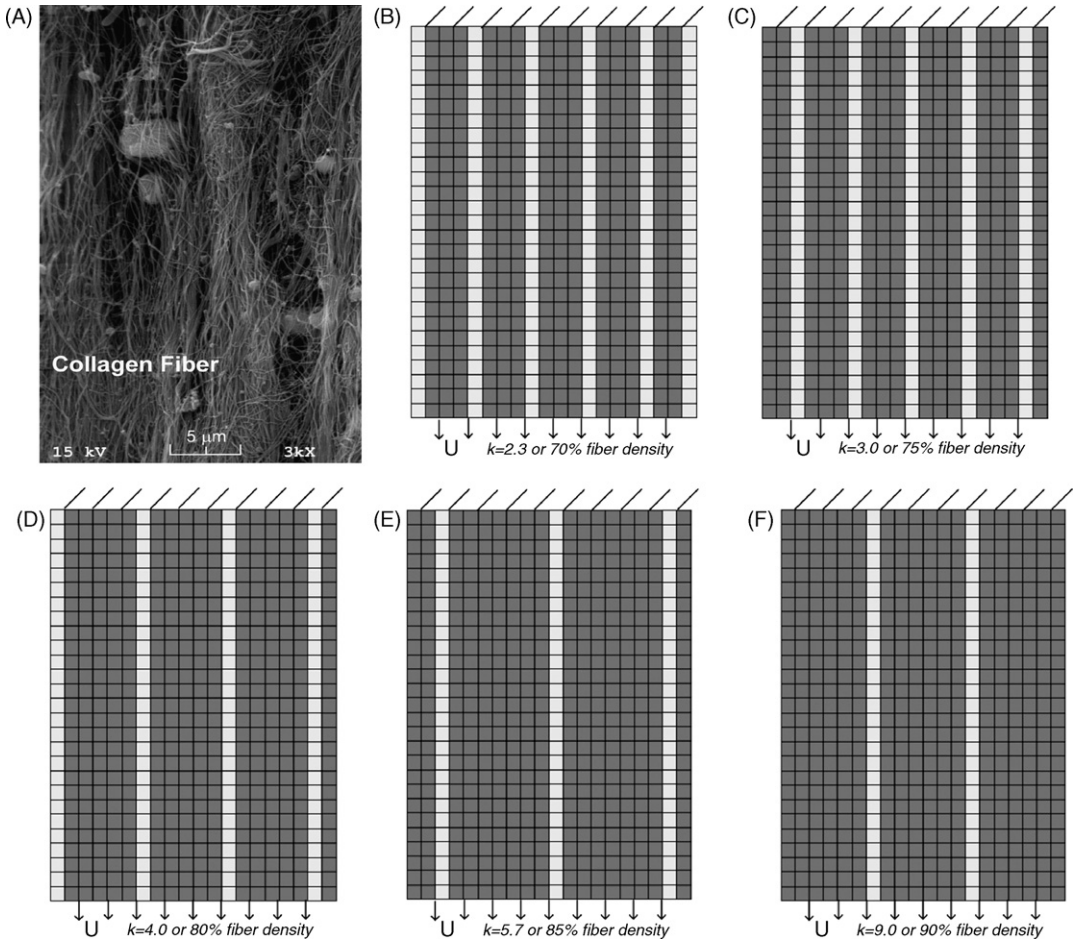

Fig. 5. (A) SEM picture of the tensor tympani tendon at 3000× magnification. (B) FE model #1 of the tensor tympani tendon with the collagen fiber-ground substance ratio k of 2.3 or fiber density of 70%. (C) FE model #2 of the tensor tympani tendon with the collagen fiber-ground substance ratio k of 3.0 or fiber density of 75%. (D) FE model #3 with the k of 4.0 or fiber density of 80%. (E) FE model #4 with the k of 5.7 or fiber density of 85%. (F) FE model #5 with the k of 9.0 or fiber density of 90%. The elements with dark color represent the collagen fibers and those with white color represent the ground substance.

Fig. 5B–F. Note that only X–Y plane models were shown for a better illustration. The length, width and thickness of each model were 1.45, 1.12 and 0.84 mm, respectively, based on mean dimensions of specimens listed in Table 1. Each model was meshed by eight-node hexahedral solid element (Solid185) with a total of 4860 elements and 5880 nodes. The tendon was assumed as transverse isotropic material with fibers oriented along the Y-axis. By using the first-order Ogden model ($N=1$), the initial Young's modulus of the fiber along Y direction for incompressible material ($\nu=0.5$) was expressed as

$$E_{Y0} = 2(1+\nu)G = 3G = 3\alpha_1\mu_1 \tag{7}$$

The initial modulus along X and Z directions are assumed as 1/10 of E_{Y0} due to transverse property of the tendon [13]. The ground substance was assumed to be isotropic material with a uniform Young's modulus of 10 kPa based on the lowest stiffness of soft tissues such as fat [22]. Boundary and loading conditions were applied through nodes on top and bottom surfaces of the model. For the uniaxial tensile test, all the nodes on the top surface were fixed, and all the nodes on the bottom surface were elongated. The elongation was accomplished by 120 substeps to reach the maximum of 0.6 mm.

Nonlinear structural analysis was carried out on FE models of the tendon to calculate the force and deformation. The nominal stress and strain along fiber direction at each substep were derived. Meanwhile, two material constants (μ_1 and α_1) were derived again from FE analysis through regression process with the experimental data. The stress–strain curves of FE tendon models with different microstructures were compared with that from experiments. The relationship between the structure and properties of the tendon was then determined.

3. Results

Comparison between the stress–stretch loading curve of a tendon specimen directly from the uniaxial tensile test (solid line) and that from the DIC method (broken line) is shown in Fig. 6. The results from two approaches are in good agreement up to the stretch ratio of 1.25. However, there is some

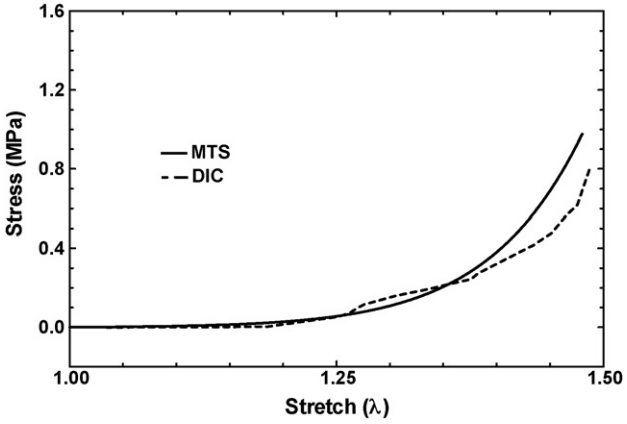

Fig. 6. Comparison of the stress–stretch curve of a tensor tympani tendon specimen obtained from DIC analysis (broken line) and MTS measurement (solid line).

deviation observed above 35% stretch (or $\lambda = 1.35$) which may be caused by the sensitivity level of the DIC method for large deformation. In MTS test, the specimen was treated as a whole unit and the grip to grip displacement was used for strain calculation. The results from DIC were relied on local micro-deformation in the tissue, which may have different response at large deformation.

Fig. 7A shows stress–stretch curves of 10 specimens under loading process. Most specimens were stretched up to λ of 1.4. Fig. 7B displays the mean and S.D. It is clearly seen that the absolute S.D. increases with the stress, while the relative S.D. remains the same at 0.12. The stress response of the tendon is almost flat at low strain level, but it stiffens rapidly after the stretch ratio λ increases above 1.2.

Through the data iteration process in MATLAB v. 7.0, two material constants, μ_1 and α_1 in Eq. (2), were determined as $\mu_1 = 0.01$ MPa and $\alpha_1 = 23.52$ using the mean experimental data of Fig. 7. Therefore, the constitutive equation of the tensor tympani tendon in the Ogden form is derived as

$$\sigma = 8.5 \times 10^{-4}(\lambda^{22.52} - \lambda^{-12.76})$$
$$\text{for } 0\,\text{MPa} \le \sigma \le 1.5\,\text{MPa}, \quad 1 \le \lambda < 1.4 \tag{8}$$

The Young's modulus of each tendon derived from Eq. (3) is plotted against the stress derived from Eq. (2) as shown in Fig. 8A. The mean Young's modulus and stress with S.D. is shown in Fig. 8B. It is clearly seen that the Young's modulus

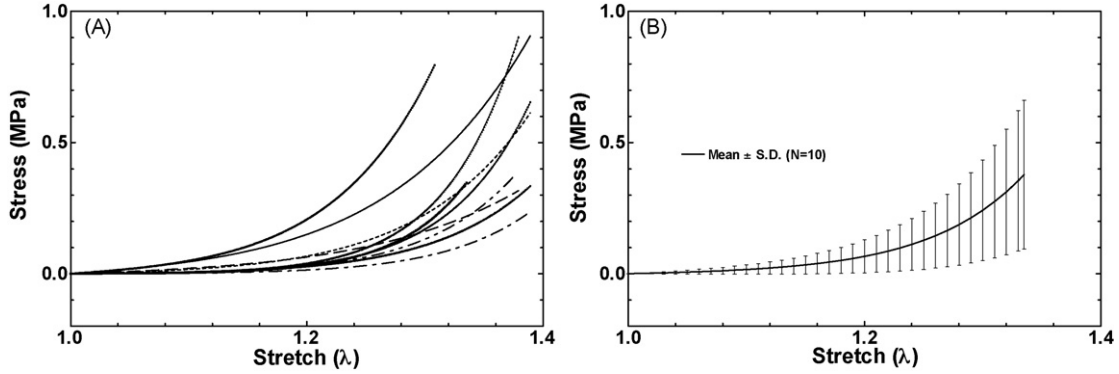

Fig. 7. (A) Stress–stretch curves of 10 tensor tympani tendon specimens under uniaxial loading processes. The maximum stretch ratio λ was around 1.4 and the elongation rate was 0.01 mm/s. (B) The mean value of stress–stretch curves of 10 tensor tympani tendon specimens with standard deviation (S.D.) bars.

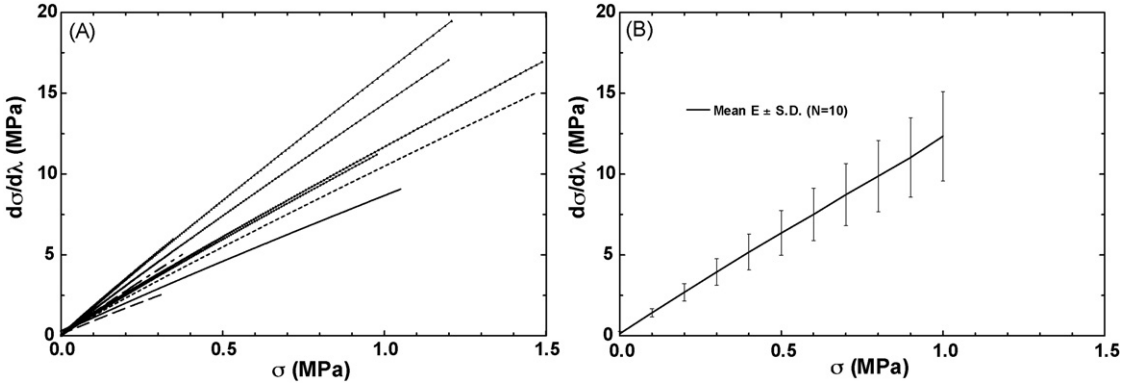

Fig. 8. (A) Young's modulus–stress curves of 10 tensor tympani tendon specimens under uniaxial loading processes. (B) The mean value of Young's modulus–stress curves of 10 tensor tympani tendon specimens with standard deviation (S.D.) bars.

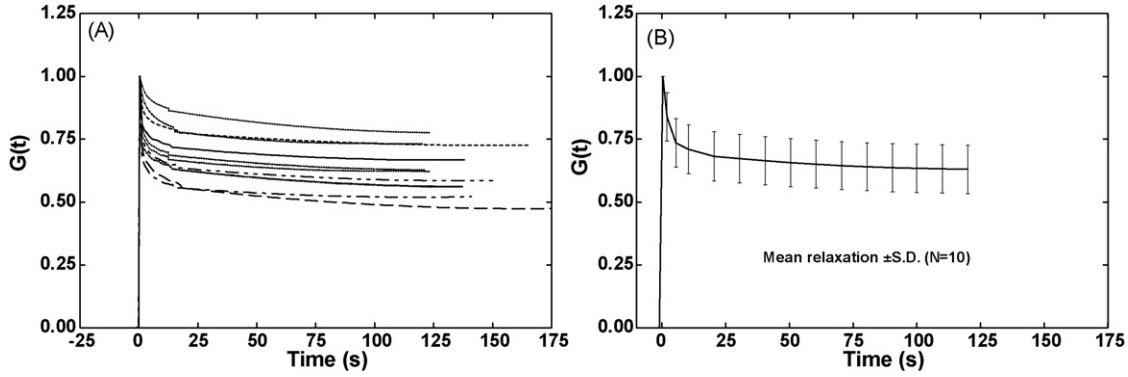

Fig. 9. (A) Normalized stress relaxation functions $G(t)$ of 10 tensor tympani tendon specimens from stress relaxation tests. (B) The mean value of $G(t)$ of 10 tensor tympani tendon specimens with standard deviation (S.D.) bars.

of the tensor tympani tendon is linearly increasing with the stress, the value varies from 0.14 to 12.34 MPa when the stress increases from 0 to 1 MPa.

Fig. 9A shows normalized stress relaxation functions of 10 tendon specimens. The stress $\sigma(t)$ decreases with time and finally reaches a stable state after 120 s. The normalized stress relaxation function $G(t)$ is defined as the ratio between stress $\sigma(t)$ and the initial stress σ_0. The mean normalized stress relaxation function $G(t)$ with S.D. is shown in Fig. 9B. The mean initial stress for 10 specimens is 1.33 MPa. Within 1 s, 21% of the stress is relaxed; after 5 s, 27% of the stress is relaxed; and finally after 120 s, 37% of the stress is totally relaxed. The mean stress after total relaxation is 0.84 MPa.

The stress–stretch ratio relationships of five FE tendon models are compared with the mean experimental data (Fig. 10). The material constants from FE analysis are listed in Table 2. It is clearly seen that the FE model #3 with the fiber density of 80% has the closest behavior as that from experiments. The material constants of the FE model #3, $\mu_1 = 0.007$ MPa and $\alpha_1 = 20$, are also close to the values obtained from experimental data.

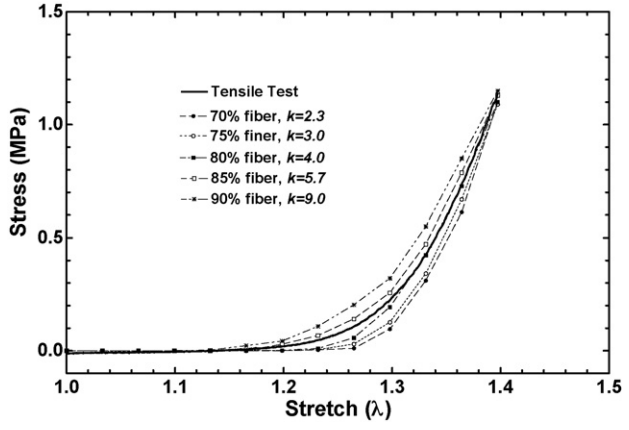

Fig. 10. Comparison between stress–stretch curves of the tensor tympani tendon obtained from FE models and the mean curve measured from 10 tendon specimens in uniaxial tensile tests. The broken lines with symbols represent modeling results from five FE tendon models. The solid line without symbols represents the experimental mean curve.

Table 2
Material constants of tensor tympani tendon (TTT) obtained from five FE models

Model #	Fiber/substance ratio, k	Fiber density (%)	μ_1 (MPa)	α_1
1	2.3	70	0.008	25
2	3.0	75	0.007	32
3	4.0	80	0.007	20
4	5.7	85	0.006	19
5	9.0	90	0.005	23

Table 3 lists the failure stress and stretch of 10 tendon specimens. The mean failure stress is 2.25 MPa with S.D. of 1.47 MPa, which shows the strength variation among tested individual specimens. The breaking location of all specimens occurred in their midsubstance.

4. Discussion

In this study, mechanical experiments were performed in tensor tympani tendon specimens. Digital image correlation method was applied to test the boundary effect on experiments. The experimental data were analyzed using the hyperelastic Ogden model to derive the stress–strain relationship (Fig. 7) and Young's modulus–stress relationship (Fig. 8). The constitutive equation (Eq. (8)) shows nonlinear elastic properties of the tensor tympani tendon for the first time in literature.

The hysteresis phenomenon is observed for the tendon with the unloading curve below the loading curve as shown in Fig. 3. The stress relaxation function is shown in Fig. 9. The results suggest that the tensor tympani tendon is a typical viscoelastic material with the constitutive behavior related to the stress and strain history. The lag of unloading curve to loading curve indicates the loss of internal energy during the deformation of the specimen. Therefore, only the loading curves were analyzed in this study.

In stress relaxation test, an elongation rate of 1.8 mm/s was used to elongate the specimen of about 0.6 mm (based on average specimen length and 40% elongation). This elon-

Table 3
Failure stress and stretch of tensor tympani tendon (TTT) specimens ($N = 10$)

	TTT1	TTT2	TTT3	TTT4	TTT5	TTT6	TTT7	TTT8	TTT9	TTT10	Mean	S.D. (±)
Failure stress (MPa)	1.61	2.06	0.98	0.58	1.55	1.81	2.65	2.98	2.38	5.88	2.25	1.47
Failure stretch, λ	1.53	1.59	1.70	1.59	1.88	1.71	1.57	1.74	1.65	1.69	1.66	0.10

gation rate is 180 times faster than the elongation rate used in tensile test (0.01 mm/s) and can be considered as a sufficiently high rate of loading. The initial stress in specimen was imposed within 0.3 s, which provided a reasonable approximation of the tensile stress generated instantaneously in the tissue [14]. However, compared with the ideal step function of stretching, the relaxation function obtained in this study would be slightly lower than that from ideality [23].

The SEM picture of a tendon specimen (Fig. 5A) shows that the tendon is mainly composed of collagen fibers embedded into ground substance matrix. However, it is difficult to calculate the fiber density of the tendon based on the picture. Therefore, five FE tendon models with varying fiber density were created to explore the relationship between the structure and properties of the tendon. The results in Fig. 10 suggest that the stress–strain curve shifts up when the fiber density increases. This indicates that the Young's modulus increases with collagen fiber density and mechanical properties of the tendon are related to the structure of the tissue. Note that collagen fibrils of the tendon was assumed straight and uniformly distributed in FE models. In reality, collagen fibrils could be crimped for some tissues [24].

The interaction between collagen fibers and ground substances would also contribute to elastic response of the tissue [25], which was not included in current study. Considering the moduli in perpendicular directions and the properties of ground substances may affect FE analysis results, we performed sensitivity studies on FE modeling (results not included) and found that the material constant μ_1 was sensitive to assumption of moduli along the perpendicular directions, and the behavior of tendon was affected by properties of ground substances. In our future studies, a FE tendon model with more accurate fiber structures will be developed and the interaction between fibers and ground substances will be included.

In summary, the results obtained from this study indicate that the tensor tympani tendon is a viscoelastic material with nonlinear stress–strain relationship. The hyperelastic Ogden model provides a good representation for non-linear behavior of the tendon. The data reported in this paper add useful information to ear tissue biomechanics through both experimental measurement and theoretical modeling analysis.

Acknowledgements

The experiment assistances from C. Dai at University of Oklahoma and D. Nakmali at Hough Ear Institute are gratefully acknowledged. This work was supported by NIH/NIDCD R01DC006632 and NSF/CMS 0510563 Grants.

References

[1] Huttenbrink KB. Movement of the ear ossicles by middle ear muscle contraction. Laryngorhinootologie 1989;68(11):614–21.
[2] Asai M, Roberson Jr JB, Goode RL. Acoustic effect of malleus head removal and tensor tympani muscle section on middle ear reconstruction. Laryngoscope 1997;107(9):1217–22.
[3] Badia L, Parikh A, Brookes GB. Management of middle ear myoclonus. J Laryngol Otol 1994;108(5):380–2.
[4] Golz A, Fradis M, Netzer A, Ridder GJ, Westerman ST, Joachims HZ. Bilateral tinnitus due to middle-ear myoclonus. Int Tinnitus J 2003;9(1):52–5.
[5] Pau HW, Punke C, Zehlicke T, Dressler D, Sievert U. Tonic contractions of the tensor tympani muscle: a key to some non-specific middle ear symptoms? Hypothesis and data from temporal bone experiments. Acta Otolaryngol 2005;125(11):1168–75.
[6] Love Jr JT, Stream RW. The biphasic acoustic reflex: a new perspective. Laryngoscope 1978;88:298–313.
[7] Bauer M, Vona I, Gerlinger I. Reconstruction of the tensor tympani tendon. J Laryngol Otol 2006;120(3):240–3.
[8] Abdelhamid MM, Paparella MM, Schachern PA, Yoon TH. Histopathology of the tensor tympani muscle in otitis media. Eur Arch Otorhinolaryngol 1990;248(2):71–8.
[9] Gan RZ, Sun Q, Feng B, Wood MW. Acoustic-structural coupled finite element analysis for sound transmission in human ear—pressure distributions. Med Eng Phys 2006;28:395–404.
[10] Quapp KM, Weiss JA. Material characterization of human medial collateral ligament. ASME J Biomech Eng 1998;120:757–63.
[11] Lanir Y, Fung YC. Two-dimensional mechanical properties of rabbit skin. I. Experimental system. J Biomech 1974;7:29–34.
[12] Gardiner JC, Weiss JA. Simple shear testing of parallel-fibered planar soft tissues. ASME J Biomech Eng 2001;123:170–5.
[13] Weiss JA, Gardiner JC. Computational modeling of ligament mechanics. Crit Rev Biomed Eng 2001;29(3):303–71.
[14] Fung YC. Biomechanics: mechanical properties of living tissues. New York, Inc.: Springer-Verlag; 1993.
[15] Weiss JA, Gardiner JC, Bonifasi-Lista C. Ligament material behavior is nonlinear, viscoelastic and rate-independent under shear loading. J Biomech 2002;35:943–50.
[16] Liu Y, Kerdok AE, Howe RD. A nonlinear finite element model of soft tissue indentation. ISMS 2004. LNCS 3078:67–76.
[17] Lu H, Cary PD. Deformation measurements by digital image correlation: implementation of a second-order displacement gradient. Exp Mech 2000;40(4):1–8.
[18] Wu JZ, Dong RG, Smutz WP, Schopper AW. Nonlinear and viscoelastic characteristics of skin under compression: experiment and analysis. Biomed Mater Eng 2003;13(4):373–85.
[19] Sarma PA, Pidaparti RM, Moulik PN, Meiss RA. Non-linear material models for tracheal smooth muscle tissue. Biomed Mater Eng 2003;13(3):235–45.
[20] Miller K, Chinzei K. Mechanical properties of brain tissue in tension. J Biomech 2002;35(4):483–90.
[21] Wang B, Lu H, Kim G. A damage model for the fatigue life of elastomeric materials. Mech Mater 2002;34:475–83.

[22] Wellman P, Howe RH, Dalton E, Kern KA Breast tissue stiffness in compression is correlated to histological diagnosis. Technical report. Harvard Biorobotics Laboratory. 1999. http://biorobotics.harvard.edu/pubs/mechprops.pdf.
[23] Doehring TC, Carew EO, Vesely I. The effect of strain rate on the viscoelastic response of aortic valve tissue: a direct-fit approach. Ann Biomed Eng 2004;32(2):223–32.
[24] Freed AD, Doehring TC. Elastic model for crimped collagen fibrils. J Biomech Eng 2005;127:587–93.
[25] Puso MA, Weiss JA. Finite element implementation of anisotropic quasi-linear viscoelasticity using a discrete spectrum approximation. J Biomech Eng 1998;120(1):62–70.